Communication

Additively Manufactured Nitrogen-Atomized 17-4 PH Stainless Steel with Mechanical Properties Comparable to Wrought

ERIC A. LASS, MARK R. STOUDT, and MAUREEN E. WILLIAMS

The microstructure of additively manufactured (AM) nitrogen-atomized 17-4 contains 12 ± 4 pct retained austenite after conventional solutionization annealing at 1323 K (1050 °C) resulting in a yield strength of about half that of wrought, which contains ≈ 100 pct BCC/martensite. An AM17-4 microstructure containing a volume fraction of ≈ 95 pct martensite is achieved by solutionizing at 1273 K (1000 °C) instead of 1323 K (1050 °C), where more nitrogen is trapped as M(C,N)-carbides, followed by further cooling to 233 K (− 40 °C). This alternative solutionization recovers the yield strength of the AM material to > 90 pct of its wrought counterpart, a critical first step toward the implementation of AM17-4 in real-world applications.

https://doi.org/10.1007/s11661-019-05124-0

Additive manufacturing (AM) of metallic materials is a potentially transformative technology because it provides a method for producing complex, three-dimensional parts with virtually unlimited design freedom. However, to date, only a handful of alloys are available for use in AM processes, and many of these materials, although weldable in wrought form, produce significant challenges when applied to AM. Of these materials, precipitation-hardenable martensitic stainless steels, specifically 17-4, are of great interest for AM applications because of their unique combination of high strength and corrosion resistance. However, successful implementation of these materials for AM-produced components has proven difficult. A significant amount of nitrogen, a well-known FCC/austenite stabilizer in steels, remains in N_2-gas-atomized 17-4 powder feedstock.[1–6] As a result, components built from such powder contain a large volume fraction of retained austenite (RA). The as-built material exhibits a yield point phenomenon in tension and compression, with an upper yield strength of 500 to 600 MPa.[1,5,6] This is significantly lower than the yield strength of wrought 17-4 (W17-4), which is typically around 1000 MPa, but can be as low as 760 MPa. Yielding is followed by a region of constant stress with increasing strain, followed by significant work hardening, An increase in the ultimate tensile strength and elongation to failure is also commonly observed in AM17-4 compared to W17-4. This is likely a result of the strain-induced transformation of austenite to martensite,[1] akin to transformation-induced plasticity in TRIP steels. Argon gas-atomized 17-4 powder provides one alternative to N_2-atomized material.[1,3,7–9] However, Ar-atomized powder is more expensive. More importantly, Ar is insoluble in steel, resulting in large amounts of trapped-gas porosity in the AM product, which is detrimental to both mechanical and corrosion behavior.[8–10] Water-atomized powder is sometimes used in traditional powder metallurgy applications,[11–13] though the powder properties are not well-suited for AM, and its investigation as feedstock for AM is limited.[14] Both Ar- and water-atomized AM17-4 material can exhibit the same unusual stress–strain behavior as observed in N_2-atomized material in the as-built condition,[7–9,14] a result of the rapid solidification conditions yielding a fraction of RA in the as-deposited microstructure. However, cast/wrought thermal processing protocol, consisting of homogenization at 1423 K (1150 °C) for 1 hour, followed by solutionization at 1323 K (1050 °C) for 30 minutes (*i.e.*, condition A (CA)), eliminates such behavior. Thermal processing of N_2-atomized AM17-4 reduces but does not eliminate this behavior, and yield strength remains about 50 pct of that typical for W17-4 in condition A. The present work demonstrates that tensile behavior similar to W17-4 can be achieved in AM17-4 produced from N_2-atomized powder, with comparable yield strength and no yield point phenomenon, through an alternative post-build thermal processing protocol.

The AM17-4 samples, 10 mm cubes, and sub-scale tensile bars were built using 17-4 powder (EOS GP1 grade[15]) using an EOS M270 laser powder-bed fusion system and a standard EOS parameter set for GP1 powder. W17-4 plate stock was also used for comparison with the AM17-4. The compositions of both W17-4 and AM17-4 materials are found in Table I, with the only significant difference being the high N-content of the AM alloy. The AM samples were cut from the build plate *via* electrical discharge machining in the as-built

ERIC A. LASS, MARK R. STOUDT, and MAUREEN E. WILLIAMS are with the Materials Science and Engineering Division, Material Measurement Laboratory, National Institute of Standards and Technology, Gaithersburg, MD, 20899. Contact e-mail: eric.lass@nist.gov

Manuscript submitted November 21, 2018.
Article published online February 4, 2019

Table I. Compositions of the W17-4 and AM17-4 Materials in Mass Fraction × 100

Element	Wrought	AM
Fe	balance	balance
Cr	15.80	15.73 ± 0.23
Ni	4.24	4.57 ± 0.08
Cu	3.32	4.01 ± 0.05
Mn	0.54	0.64 ± 0.04
Nb	0.30	0.27 ± 0.02
Si	0.40	0.76 ± 0.03
C	0.04	0.04 ± 0.01
N	0.03	0.12 ± 0.01
P	0.021	0.007 ± 0.001
S	0.001	0.004 ± 0.000

Only one W17-4 measurement was performed. Specimens were sent to an independent laboratory for compositional analysis according to ASTM standards.

condition. All samples were sealed in evacuated and Ar-backfilled quartz ampules for heat treatment. The encapsulated AM samples were first homogenized at 1423 K (1150 °C) for 1 hour[4,16] followed by quenching in room temperature water without breaking the quartz (no-break quench, NBQ), resulting in a quench rate roughly equal to air cooling, reaching room temperature in tens of seconds. The homogenized samples were then solutionized for 1 hour at temperatures between 1248 K and 1323 K (975 °C and 1050 °C), and for 30 minutes at 1323 K (1050 °C) (condition A, AM-CA), followed by a NBQ. Some of the heat-treated samples were further cooled in a methanol bath to temperatures between 273 K and 213 K (0 °C and − 60 °C) and held at temperature for 30 minutes. Samples of W17-4 were also encapsulated and solutionized for 30 minutes at 1323 K (1050 °C) then NBQ (W-CA) for comparison. The AM samples are designated by the annealing temperature and whether they were further quenched. That is, ''AM-1000-Q'' was annealed at 1273 K (1000 °C) for 1 hour followed by NBQ, then further quenched to subzero [233 K (− 40 °C) unless otherwise stated].

The samples were mounted and polished to a 1 μm finish using standard metallographic techniques, followed by etching *via* immersion in Kallings #1 (225 mL ethanol, 20 mL HCl, 12 g $CuCl_2$) for 10 to 20 seconds to reveal the microstructure. Optical microscopy (OM), scanning electron microscopy (SEM), and energy dispersive X-ray spectroscopy (EDS) were employed for microstructural analysis. Laboratory-based X-ray diffraction (XRD) analysis was performed on polished specimens using Cu K_α radiation using a scan range of 40 to 50 deg 2θ to focus on the relative intensities of FCC (111) and BCC (110) reflections. The volume fractions of austenite and BCC/martensite (hereafter referred to simply as ''fraction'') were estimated from the measured relative intensities of these two peaks, using the direct comparison method given in Reference 17, the same method used by Meredith *et al.*[3] Crystallographic texture was found not to bias the RA fraction measurements in the heat-treated samples. This is because the many variants of the martensite-austenite orientation relationship, combined with the recrystallization that occurs during the homogenization/solutionization process (a result of residual stresses/strains in the as-built material and of the plastic deformation imparted by the martensitic transformation in previously heat-treated material), creates a random average grain orientation in the heat-treated samples. This was confirmed by multiple scans on the same sample with different rotations with respect to the incident beam, which yielded RA fractions within 1 pct of each other. The as-built material did exhibit some texture-related change in the measured RA fraction. Samples measured with the incident beam quasi-parallel to the build direction yielded measured RA fractions 5 to 10 pct higher than those measured quasi-perpendicular to the build direction.

Because of the deformation-induced austenite to martensite transformation in AM17-4, it is possible that the thin deformation layer on the sample surface may give rise to increased uncertainty in the measured RA fraction. However, EBSD measurements suggest this damage layer is ≈ 1 μm, determined by changing the accelerating voltage of the SEM, and consequently, the depth of penetration of the electron beam, which has a penetration depth on the order of a few micrometers. Preliminary synchrotron-based XRD experiments also show agreement with the laboratory-based results presented here[18] and will be included in a future report. Regardless, to account for the possible errors associate with this deformation layer, the uncertainty in the phase fractions is given as ± 20 pct of the measured value, which represents approximately four times the standard deviation of measurements.

The Thermo-Calc software[19] and TCFE8 thermodynamic database[20] were employed to calculate phase equilibria, including phase fractions and compositions. The Ghosh and Olson model for calculating martensite start temperature, M_s,[21,22] based on the theory of martensite nucleation developed by Olson and Cohen,[23–25] was also employed to calculate the effects of nitrogen content and solutionization temperature on M_s.

Tensile samples with 2.5 mm nominal thickness were parallel-sliced by EDM from additively manufactured 140 mm × 12 mm dog bone-shaped blocks. The gauge section of the specimen was 25 mm length by 6.5 mm wide. The tensile axis for these specimens was perpendicular to the build plane (*i.e.*, parallel to the *x*-*y* plane). These specimens were annealed to the aforementioned AM-CA and AM-1000-Q conditions. An additional set of tensile specimens was cut by waterjet from 3-mm-thick W17-4 plate stock with the tensile axis parallel to the rolling direction. These specimens were heat treated to the W-CA condition. All uniaxial tensile tests were performed using a strain rate of 2.5×10^{-4} s^{-1}. Two or three tensile specimens were tested for each condition, except for the as-built, to provide statistical information.

Figure 1 shows the microstructures of the W-CA and AM-CA materials. Both microstructures exhibit a plate-like martensitic microstructure when observed *via* OM, with the average plate width of the AM material being smaller, looking more lath-like, compared to that

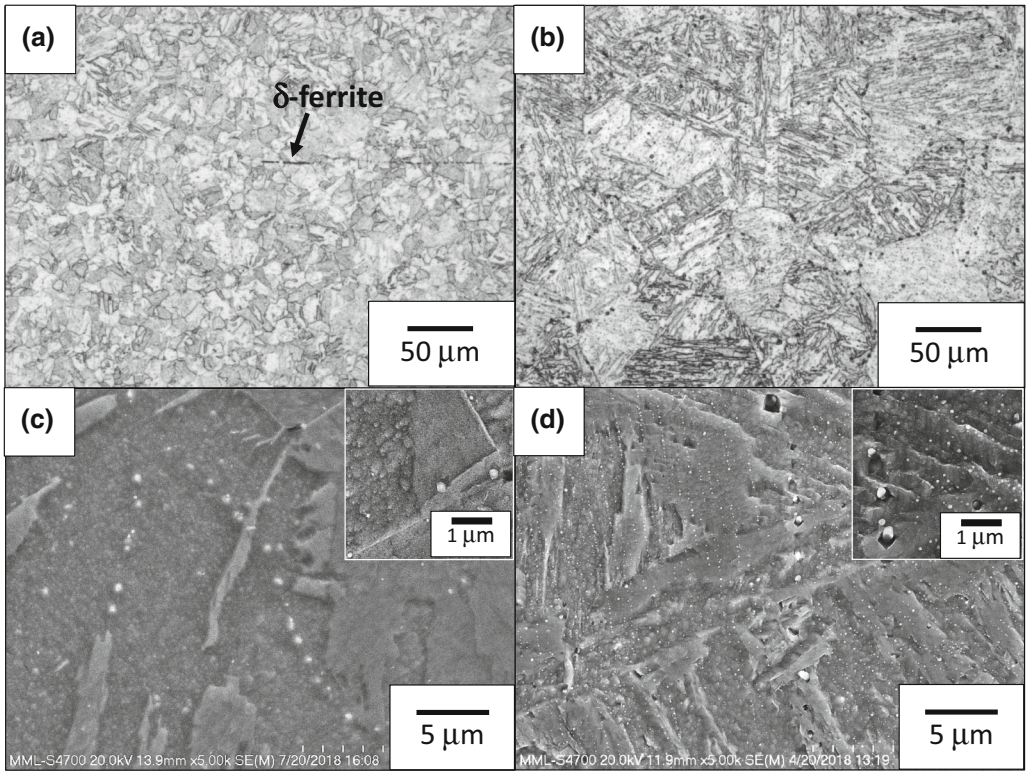

Fig. 1—Optical micrographs of (*a*) W17-4 and (*b*) (homogenized) AM17-4 after solutionization at 1323 K (1050 °C) for 30 min, and SEM micrographs of the same (*c*) W17-4 and (*d*) AM17-4 samples.

found in the wrought sample. The wrought material also contains "stringers" of δ-ferrite, shown as dark streaks in Figure 1(a). When viewed using SEM, both materials are found to contain precipitates several hundreds of nanometers in diameter (bright particles in Figures 1(c) and (d)) along prior austenite grain boundaries. The AM17-4 sample also contains a fine dispersion of intragranular precipitates with an average diameter < 100 nm, which are not present in the wrought material. These precipitates are sometimes found in linear arrays (Figure 1(d) inset), tracing the prior interdendritic regions of the as-solidified microstructure. EDS analysis confirms both populations are rich in Nb, consistent with Cheruvathur *et al.*,[4] who identified the precipitates as M(C,N)-type carbides. The fine precipitates are found exclusively in the heat-treated AM material, and are observed regardless of the solutionizing temperature or time. In addition to Nb, they are likely enriched in N, which readily substitutes for C in M(C,N) carbide. These fine intragranular precipitates may be at least partially responsible for the decreased plate thickness of the martensite found in the AM17-4 material, impeding the dislocation motion required for martensite-austenite interfacial motion.[23–25]

Figure 2(a) presents the XRD results for as-built AM17-4, AM-CA, and W-CA. The as-built material contains a significant RA fraction, estimated to be 35 ± 14 pct. After homogenization, the RA fraction is reduced significantly, to 12 ± 4 pct, though this is still quite high compared to the wrought material, which is nearly 100 pct BCC/martensite according to the XRD results. The primary reason for RA in the AM material is the high concentration of austenite-stabilizing N, arising from N_2 gas used during gas atomization of the powder feedstock. The calculated M_s of AM17-4 (with a mass fraction of N of 0.12 pct) after solutionizing at 1323 K (1050 °C) is 387 K (114 °C), with an equilibrium volume fraction (estimated as the calculated mole fraction) of M(C,N) carbides of 0.54 pct; while if the N-content is zero, the calculated M_s is 440 K (167 °C) with 0.22 pct M(C,N). Therefore, the N-content decreases M_s by > 50 K (50 °C). The martensite finish temperature, M_f, is also expected to decrease as M_s decreases, leaving more RA at room temperature. As mentioned above, this high fraction of RA in AM17-4 negatively affects mechanical properties. Therefore, for an AM17-4 component to replace a wrought component, the RA fraction must be decreased or eliminated altogether. Two potential techniques to reduce the RA fraction are (1) quenching to lower temperatures, driving the transformation toward completion at M_f, and (2) removing the N from the FCC/austenite prior to the martensite transformation, thus stabilizing the martensite relative to the austenite. The latter can be accomplished by reducing the solutionization temperature, trapping the N in M(C,N) carbides whose equilibrium volume fraction increases as temperature is decreased. For example, the calculated M(C,N) fraction for the AM17-4 alloy annealed at 1273 K (1000 °C) is 0.61 pct (a small fraction of M_2(C,N) (0.02 pct) is predicted to form as well). This results in a decrease in the mass fraction of N in the austenite phase at the

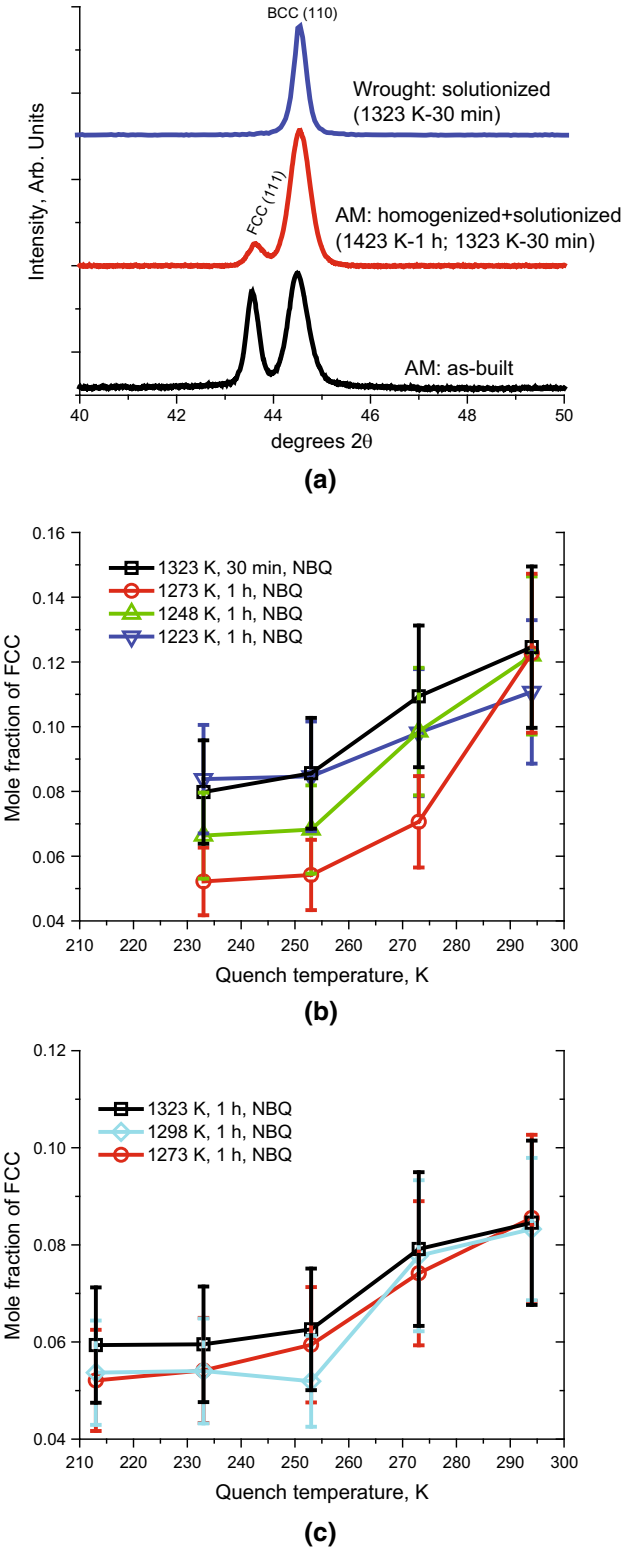

Fig. 2—(*a*) XRD patterns for W17-4, as-built AM17-4, and homogenized/solutionized AM17-4, and the measured retained austenite fraction as a function of solutionization conditions and final quench temperature for the (*b*) first and (*c*) second set of experiments.

solutionization temperature from 0.064 pct at 1323 K (1050 °C) to 0.054 pct at 1273 K (1000 °C).

Figure 2(b) shows the RA fraction in AM17-4 as a function of final quench temperature for four AM solutionization temperatures between 1223 K and 1323 K (950 °C and 1050 °C). It should be noted that thermodynamic calculations suggest that the FCC-Cu phase, *i.e.,* the precipitation strengthening phase, becomes stable at 1258 K (985 °C). Thus, 1223 K and 1248 K (950 °C and 975 °C) are not practical solutionization temperatures but are included to elucidate trends in the martensite transformation with decreasing solutionizing temperature. Figure 2(b) shows that all four samples contain the same 10 pct to 14 pct RA fraction after the NBQ. However, when cooled to lower temperatures, the AM-1000-Q sample clearly exhibits the lowest RA fraction of all conditions, < 6 pct. When quenched in liquid nitrogen, 77 K (− 196 °C), and held for 1 hour, the AM-1000-Q sample shows no further decrease in RA fraction, suggesting that M_f corresponds to about 95 pct BCC/martensite, not 100 pct, and occurs at $\approx$ 253 K (− 20 °C).

To confirm the optimal solutionization temperature for RA minimization, three additional samples, a second AM-1000-Q, AM-1025-Q, and AM-1050-Q, are presented in Figure 2(c). The RA fraction for all samples are again the same after the NBQ, about 9 pct, slightly lower than the first set of experiments. This discrepancy may be caused by local variations in processing conditions of the samples or by differences in the "damage layer" depth arising from surface preparation (*i.e.,* strain-induced transformation). However, the differences are small (within the uncertainty of the measurements), and the results of both sets of experiments clearly indicate that the RA fraction is reduced with decreasing temperature for all solutionization conditions and reaches a minimum at $\approx$ 253 K (− 20 °C). Figures 2(b) and (c) suggest that an optimal solutionization temperature exists between 1273 K and 1298 K (1000 °C and 1025 °C), where the lowest achievable RA fraction is $\approx$ 5 pct.

The tensile mechanical properties measured for W-CA, AM-CA, and AM-1000-Q are given in Table II. Typical W17-4 properties[26,27] and those from one test of the as-built material are also included for reference. The properties of W-CA are consistent with W17-4 in condition A. By comparison, both the yield stress and the ductility (strain to failure, STF, and reduction in area ratio, RAR) of the AM material in condition A (AM-CA) are substantially lower than the wrought values. Furthermore, the yield stress in this heat treatment is equal to that of the as-built condition. Looking at the AM-1000-Q, the yield stress in this condition is > 90 pct of the wrought value, although the ductility is again somewhat lower.

Figure 3(a) presents representative engineering stress–strain curves for the W-CA, AM-CA, and AM-1000-Q conditions. The W-CA curve shown in Figure 3(a) reveals that more than 50 pct of the overall strain occurs after the ultimate stress is reached, generating a pronounced necking region in those specimens during the test, and is consistent with the ductility values in Table II. In contrast, neither the AM-CA or AM-1000-Q exhibits a similar necking behavior. The

Table II. Mechanical Properties of W-CA, AM-CA, and AM-1000-Q Tensile Specimens

Sample	Yield (MPa)	Ultimate (MPa)	Elong. (× 100)	RAR (× 100)
W-CA (typical)	760 to 1000	1030 to 1103	5.0 to 8.0	N/A
W-CA	824 ± 9	1121 ± 8	10.0 ± 0.5	68.8 ± 5.9
AM-AB	452	1119	15.2	51.3
AM-CA	454 ± 5	1209 ± 2	7.8 ± 2.7	14.8 ± 5.6
AM-1000 + Q	753 ± 11	1240 ± 16	8.1 ± 0.5	23.7 ± 12.7

Because of the limited number of samples for each condition (2–3) the uncertainties are expressed as only one standard deviation. Only one as-built (AB) sample was tested so no uncertainty is given. Typical wrought values are from Refs. [26] and [27].

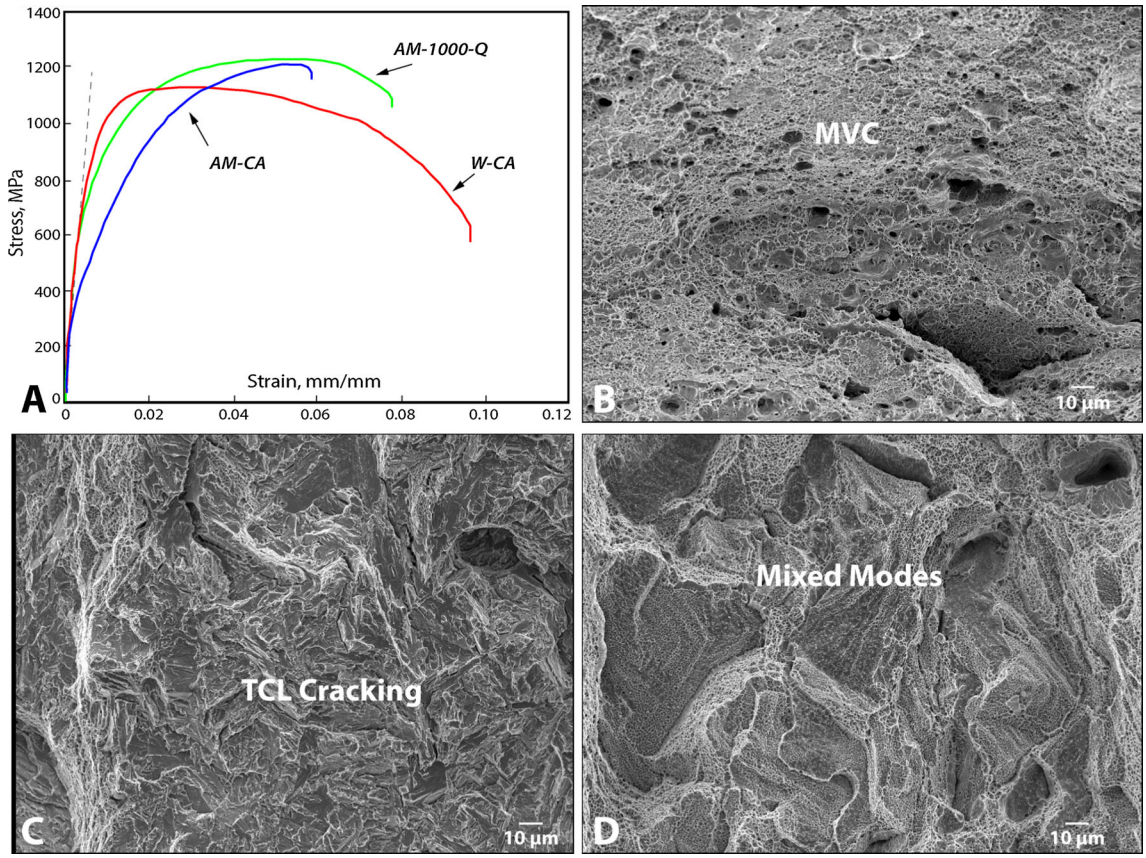

Fig. 3—(*a*) Representative tensile engineering stress–strain curves for W-CA, AM-CA, and AM-1000-Q and fractographs of each: (*b*) W-CA, (*c*) AM-CA, and (*d*) AM-1000-Q.

AM-CA specimens fail almost immediately upon reaching the ultimate stress with no observed necking, and while they exhibit better ductility than the AM-CA specimens, the AM-1000-Q specimens also do not produce a pronounced neck. The ultimate strengths for both AM conditions are similar and slightly higher than the wrought values, which may be a result of the high density of fine MC carbides and/or the high N-content of the martensite.

Representative fractographs taken from the surfaces of the W-CA, AM-CA, and AM-1000-Q are shown in Figures 3(b) through (d). The surface of the wrought material (Figure 3(b)) is composed entirely of microvoid coalescence (MVC). That is, no cracking is observed anywhere on the surface, which is consistent with the high ductility exhibited. Figure 3(c) shows the surface of the AM-CA condition. While some MVC is observed, the surface is primarily large regions of transgranular cleavage-like cracking (TCL). Such features are expected because of the limited ductility. The surface of the AM-1000-Q (Figure 3(d)) exhibits a mixture of failure modes. The primary failure in this condition is intergranular decohesion; however, further analysis reveals that the faceting in the figure also exhibits substantial amounts of fine MVC. This suggests that although failure occurs by intergranular decohesion, the individual grain boundary regions retain excellent localized fracture toughness. In addition, the prior austenite grain

size of the AM material is significantly larger than what is observed in the wrought (Figure 1), possibly giving rise to the differences in failure mode, as well as the slightly decreased yield strength of AM-1000-Q compared to W-CA.

To summarize, an alternative post-build thermal processing protocol, consisting of (1) a homogenization heat treatment of 1 hour at 1423 K (1150 °C) followed by NBQ; (2) a solutionization heat treatment of 1 hour at 1273 K (1000 °C) followed by NBQ; and (3) cooling to 233 K (− 40 °C) and holding for 30 minutes, was developed for N_2 gas-atomized AM17-4 material, which produces a microstructure consisting of 95 pct martensite, and only about 5 pct RA. The resulting material exhibits a tensile yield strength of > 90 pct of W17-4 in condition A, compared to the AM17-4 in the as-built and AM-CA conditions, which both possessed yield strength of only about 55 pct of W-CA. Further, a change in the failure mode was observed from TLC in the AM-CA to a mixed mode containing MVC in AM-1000-Q, more similar to that observed in W-CA. This is a critical step toward successful replacement of W17-4 with AM17-4 in application. It should be noted that the present results are for an alloy containing 0.12 pct N, which is typical of N_2-atomized 17-4 powders, but not the highest observed (≈ 0.15 pct N[4]). Thus, it is possible that for higher N-contents, the 95 pct martensite microstructure, and resulting > 90 pct of wrought yield strength, may not be attainable. Regardless, now that a suitable "condition A" microstructure can be obtained in N_2-atomized AM17-4, investigation of precipitation behavior is a practical next step, followed by property characterization in precipitation-hardened conditions, and finally performance evaluation in real-world applications.

The authors would like to thank the Engineering Laboratory at NIST for providing the as-built AM 17-4 samples.

REFERENCES

1. T.L. Starr, K. Rafi, B. Stucker, C.M. Scherzer, *23rd Annual Solid Freeform Fabrication Symposium*, 2012, pp. 439–46.
2. L.E. Murr, E. Martinez, J. Hernandez, S. Collins, K.N. Amato, S.M. Gaytan, and P.W. Shindo: *J. Mater. Res. Technol.*, 2012, vol. 1, pp. 167–77.
3. S.D. Meredith, J.S. Zuback, J.S. Keist, and T.A. Palmer: *Mater. Sci. Eng. A*, 2018, vol. 738, pp. 44–56.
4. S. Cheruvathur, E.A. Lass, and C.E. Campbell: *JOM*, 2016, vol. 68, pp. 930–42.
5. B. Clausen, D.W. Brown, J.S. Carpenter, K.D. Clarke, A.J. Clarke, S.C. Vogel, J.D. Bernardin, D. Spernjak, and J.M. Thompson: *Mater. Sci. Eng. A*, 2017, vol. 696, pp. 331–40.
6. W.E. Luecke and J.A. Slotwinski: *J. Res. Natl. Inst. Stand. Tech.*, 2014, vol. 119, pp. 398–418.
7. L. Facchini, N. Vicente, Jr, I. Lonardelli, E. Magalini, P. Robotti, and A. Molinari: *Adv. Eng. Mater.*, 2010, vol. 12, pp. 184–8.
8. M. Mahmoudi, A. Elwany, A. Yadollahi, S.M. Thompson, L. Bian, and N. Shamsaei: *Rapid. Proto. J.*, 2017, vol. 23, pp. 280–94.
9. A. Yadollahi, N. Shamsaei, S.M. Thompson, and L. Bian: *Int. J. Fatigue*, 2017, vol. 94, pp. 218–35.
10. M.R. Stoudt, R.E. Ricker, E.A. Lass, and L.E. Levine: *JOM*, 2017, vol. 69, pp. 506–15.
11. Y. Wu, D. Blaine, B. Marx, C. Schlaefer, and R.M. German: *Metall. Mater. Trans. A*, 2002, vol. 33A, pp. 2185–94.
12. H.Ö. Gülsoy, S. Özbek, and T. Bayakara: *Powder Metall.*, 2007, vol. 50, pp. 120–26.
13. J. Kazoir, A. Szewczyk-Nykiel, T. Pieczonka, M. Hebda, and M. Nykiel: *Adv. Mater. Res.*, 2013, vol. 811, pp. 87–92.
14. T. LeBrun, T. Nakamoto, K. Horikawa, and H. Kobayashi: *Mater. Design*, 2015, vol. 81, pp. 44–53.
15. Mention of commercial products does not imply endorsement by the National Institute of Standards and Technology, nor does it imply that such products or services are necessarily the best available for the purpose.
16. Aerospace Material Specification 5355J, "Steel, Corrosion Resistant, Investment Castings, 16Cr-4.1Ni-0.28Nb-3.2Cu, Homogenization and Solution Heat Treated or Homogenization, Solution, and Precipitation Heat Treated", SAE Aerospace, SAE International, 2009.
17. B.D. Cullity: *Elements of X-ray Diffraction*, 2nd ed., Addison-Wesley Publishing Company Inc, Philippines, 1978, pp. 411–5.
18. E.A. Lass, M.R. Stoudt, F. Zhang, unpublished research, National Institute of Standards and Technology, 2018.
19. Thermo-Calc: *Themo-Calc Software AB*, Stockholm, Sweden, 2018, p. 2018.
20. TCFE8 Fe-based superalloy database: *Themo-Calc Software AB*, Stockholm, Sweden, 2016.
21. G. Ghosh and G.B. Olson: *Acta Metall. Mater.*, 1994, vol. 42, pp. 3361–70.
22. G. Ghosh and G.B. Olson: *Acta Metall. Mater.*, 1994, vol. 42, pp. 3371–9.
23. G.B. Olson and M. Cohen: *Metall. Trans. A*, 1976, vol. 7A, pp. 1897–1904.
24. G.B. Olson and M. Cohen: *Metall. Trans. A*, 1976, vol. 7A, pp. 1905–14.
25. G.B. Olson and M. Cohen: *Metall. Trans. A*, 1976, vol. 7A, pp. 1915–23.
26. AK Steel Product Data Bulletin: *17-4 PH®* Stainless Steel, AK Steel Corporation, West Chester, OH, USA, 2016.
27. ATI Technical Data Sheet: *ATI 17-4™*, Allegheny Technologies Incorporated, Pittsburgh, PA, USA, 2016.